Supplementary Information

Selectively Plasmon-Enhanced Second-Harmonic Generation from Monolayer Tungsten Diselenide on Flexible Substrates

Zhuo Wang[1,2,3, ⊥], Zhaogang Dong[4,⊥], Hai Zhu[5,⊥], Lei Jin[6], Ming-Hui Chiu[7], Lain-Jong Li[7], Qing-Hua Xu[5], Goki Eda[2,5,8], Stefan A. Maier[3,9], Andrew T. S. Wee[1,2,8]*, Cheng-Wei Qiu[1,6,8]*, Joel K. W. Yang[4,10,]*

[1]NUS Graduate School for Integrative Sciences & Engineering (NGS), National University of Singapore, 28 Medical Drive, Singapore117456, Singapore

[2]Department of Physics, National University of Singapore, 2 Science Drive 3, Singapore 117542, Singapore

[3]Department of Physics, Imperial College London, London SW7 2AZ, UK

[4]Institute of Materials Research and Engineering, A*STAR (Agency for Science, Technology and Research), 2 Fusionopolis Way, #08-03 Innovis, Singapore 138634, Singapore

[5]Department of Chemistry, National University of Singapore, 3 Science Drive 3, Singapore 117543, Singapore

[6]Department of Electrical and Computer Engineering, National University of Singapore, 4 Engineering Drive 3, Singapore 117583, Singapore

[7]Physical Science and Engineering Division, King Abdullah University of Science and Technology, Thuwal 23955–6900, Kingdom of Saudi Arabia

[8]Centre for Advanced 2D Materials, National University of Singapore, 2 Science Drive 3, Singapore 117542

[9]Chair in Hybrid Nanosystems, Faculty of Physics, Ludwig-Maximilians-Universität München, 80799 Munich, Germany

[10]Singapore University of Technology and Design, 8 Somapah Road, Singapore 487372, Singapore

To whom correspondence should be addressed: J. K. W.Yang (joel_yang@sutd.edu.sg), C. W. Qiu (chengwei.qiu@nus.edu.sg) and A. T. S. Wee (phyweets@nus.edu.sg)
[⊥]*These authors contributed equally.*

Supplementary Figures

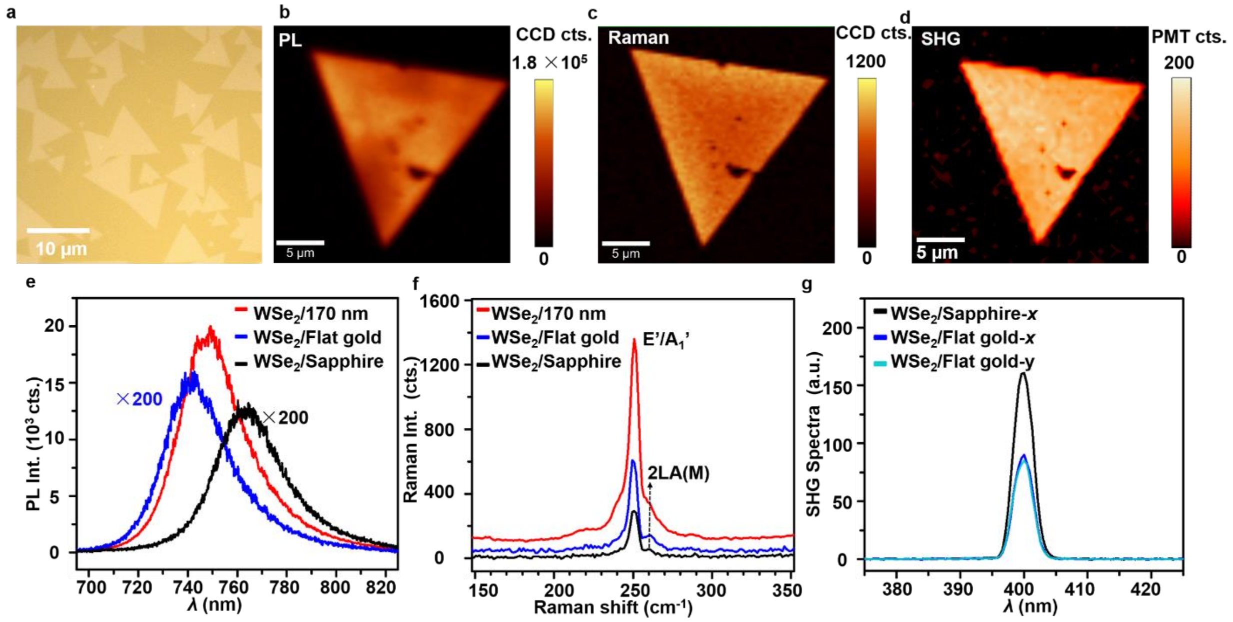

Figure S1. Characterization results of WSe_2 on sapphire, flat gold and the gold trenches. (a) Optical microscope image of WSe_2 grown on a sapphire substrate. (b)-(c) PL, Raman and SHG mappings of a triangular-shape WSe_2 on the sapphire substrate. The intensity value at each pixel for PL mapping was obtained by integrating the PL spectrum across the spectrum window of 700 − 820 nm, for Raman was the spectrum window of 245 – 265 cm^{-1} and for SHG was the peak intensity at 400 nm. The PL and Raman were measured by 532-nm CW laser, and SHG was measured by 800-nm fs laser. (e-g) Comparison of PL, Raman and SHG spectra from WSe_2 on different substrates. There is ~ 280-fold enhancement for the PL emission from WSe_2 on gold trenches as compared with WSe_2 on flat gold without normalization of the trench occupation. This is attributed to enhanced Purcell factor[S1-3], given that the PL emission at 750 nm is close to the lateral gap plasmon resonance of ~ 850 nm. *x* and *y* denote the polarization of the pump laser perpendicular and parallel to the trench orientation, respectively.

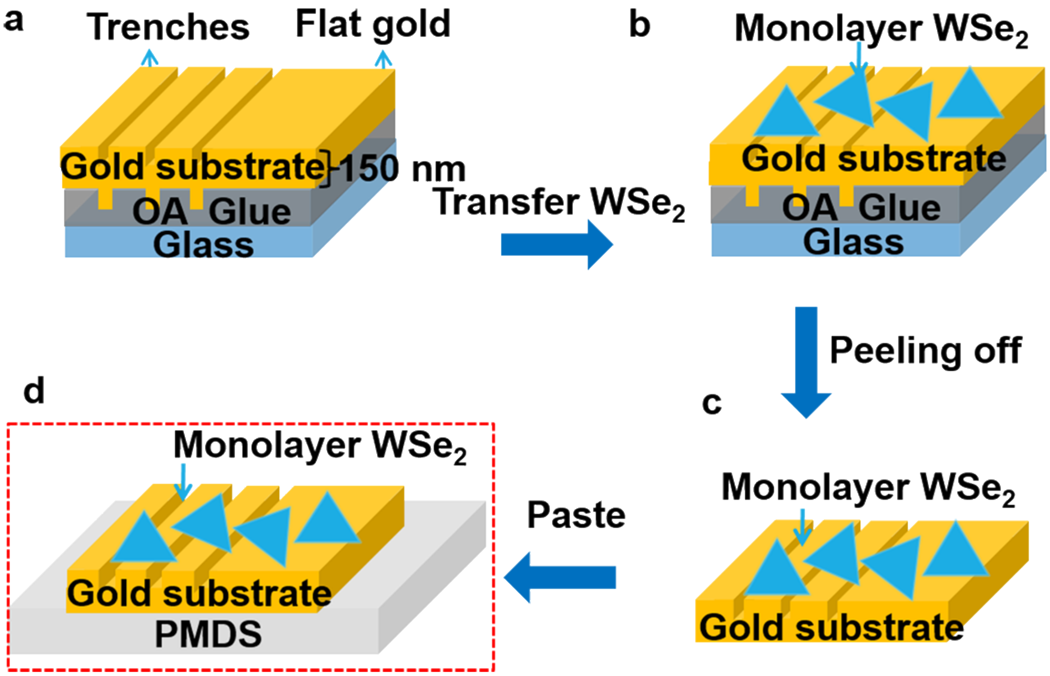

Figure S2. Detailed illustration on the fabrication processes of flexible hybrid structure. (a) Gold substrate consisting of trenches and flat gold film was prepared by template-stripping process.[S1, 4] (b) Transferring monolayer WSe_2 on gold substrate by wet transfer method. [S1] (c) Peeling off the gold substrate with WSe_2 from the glass slide by a tweezer. The gold substrate can be easily peeled off from the glass slide. (d). Adherence of the gold substrate with WSe_2 onto a flexible polydimethylsiloxane (PDMS) substrate. The gold substrate can adhere to the PDMS easily as the PDMS itself is sticky.

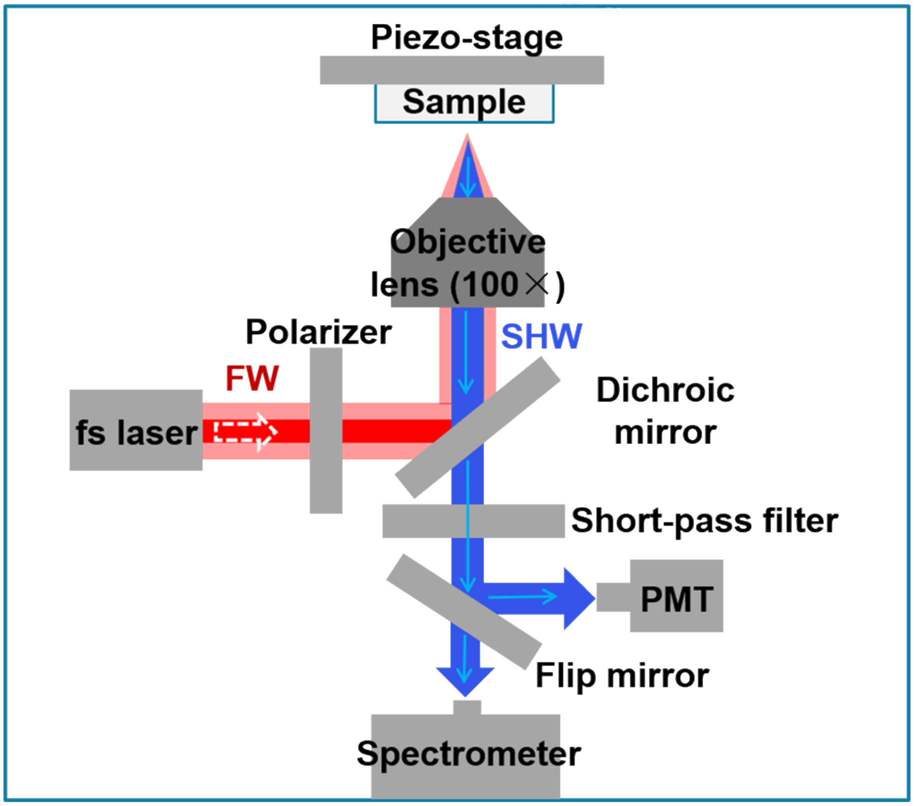

Figure S3. Optical setup for measuring SHG mappings and SHG spectra at room temperature. A femtosecond laser with a tunable central wavelength of 800 - 900 nm, pulse duration of 140 fs and repetition rate of 80 MHz, was generated from a Ti: sapphire oscillator (Coherent, Chameleon Ultra Ⅱ). This fundamental-wave (FW) laser was linearly polarized *via* a polarizer. Then it was reflected by a dichroic mirror (Semrock, FF750-SDi02-25×36) and focused on the sample through a 100× air objective with a numerical aperture (NA) of 0.90 (Nikon, Ti-U inverted microscope, TU Plan Fluor). The sample was mounted on a piezo-actuated 3D nanopositioning stage (Physik Instrumente, P545.2R7). The generated second-harmonic wave (SHW) was then back collected by the same objective and passed through the dichroic mirror. Next, the SHW went through a short pass filter (Laser 2000, FF01-750/SP-25) that was used to completely filter out the FW laser. Finally, a flip mirror was used to redirect the SHW to either a photomultiplier tube (PicoQuant, PMA 182) for SHG mappings or a spectrometer (Princeton Instruments, 2300i) for spectra measurement.

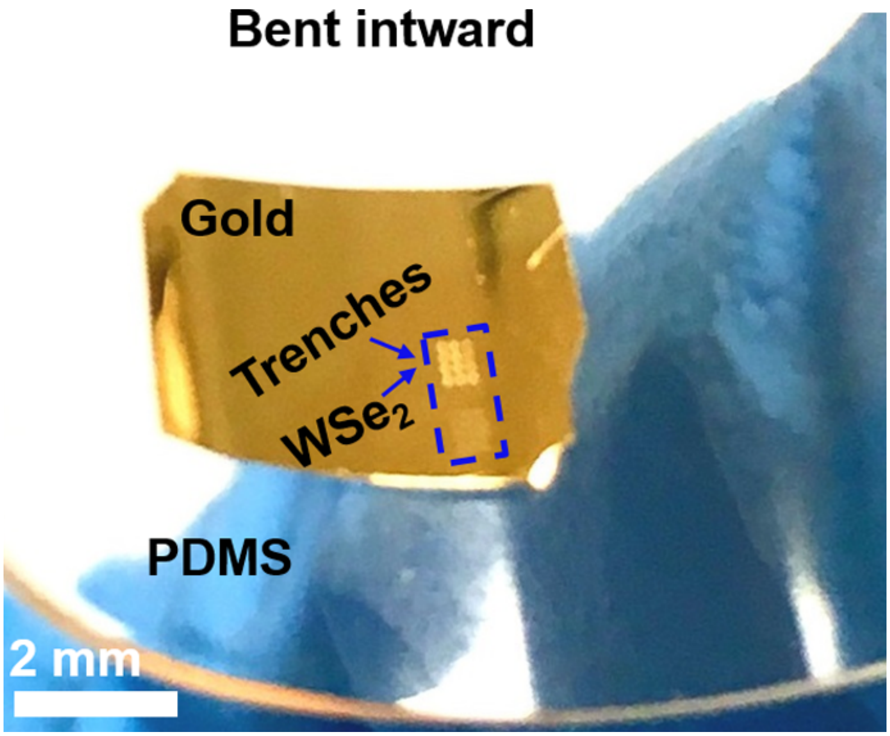

Figure S4. Photograph of WSe_2 on a gold substrate attached to an inward-bent polydimethylsiloxane (PDMS) substrate. Monolayer WSe_2 was transferred onto a region with gold trenches and flat gold film as outlined in blue dashed lines.

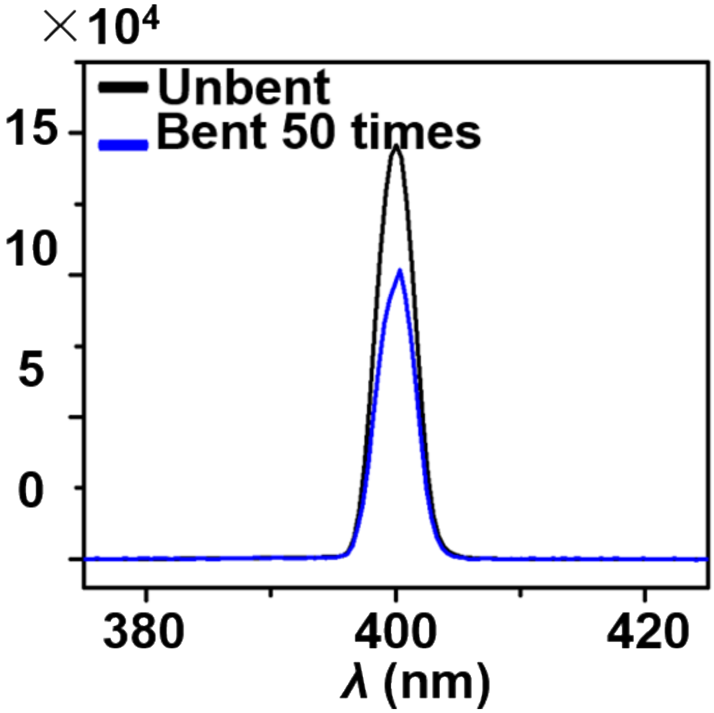

Figure S5. SHG spectra of the sample (WSe_2 on trenches with a pitch of 170 nm) before and after being bent 50 times

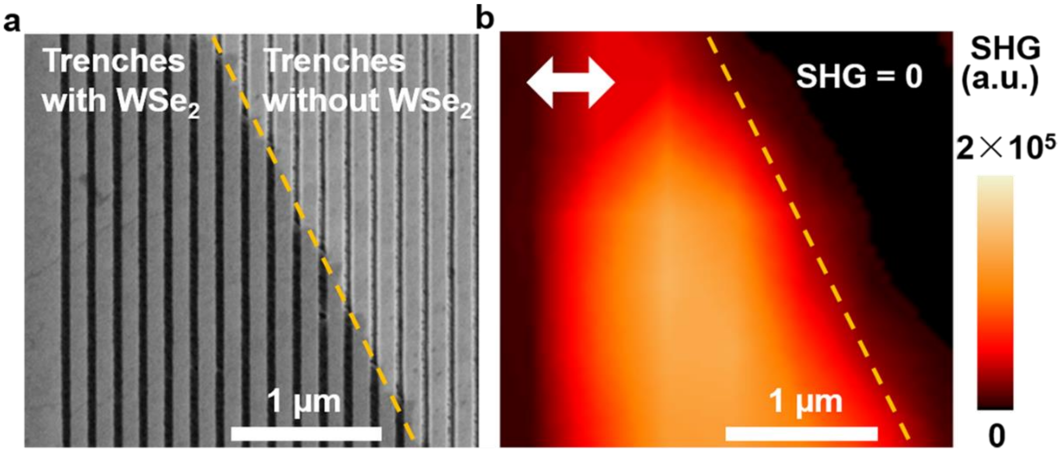

Figure S6. Gold trenches without WSe$_2$ has no SHG. (a) SEM image of gold trenches with and without WSe$_2$ and the associated SHG mapping (b). The gold trenches have a pitch of 170 nm. The yellow dashed line outlines the boundary of the gold trenches with and without WSe$_2$.

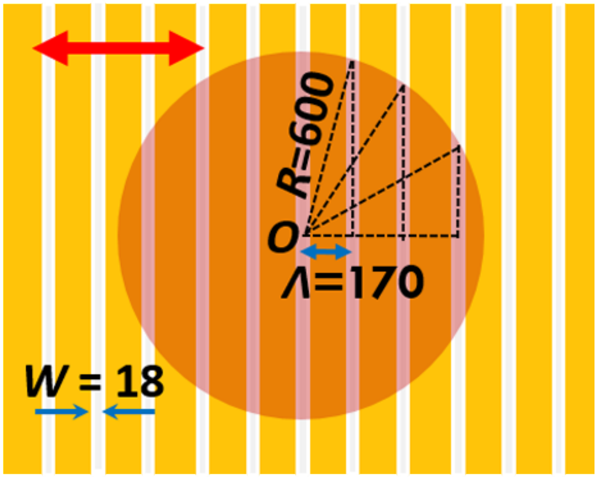

Figure S7. Diagram showing the area of multiple trenches perpendicular to the polarization direction of the laser within a laser spot. The red arrow denotes the polarization direction of the laser and the red circle represents the laser spot. *Λ* denotes the pitch size and *W* denotes the trench width. The dashed lines illustrate how Pythagorean theorem was used to calculate the length of the trenches.

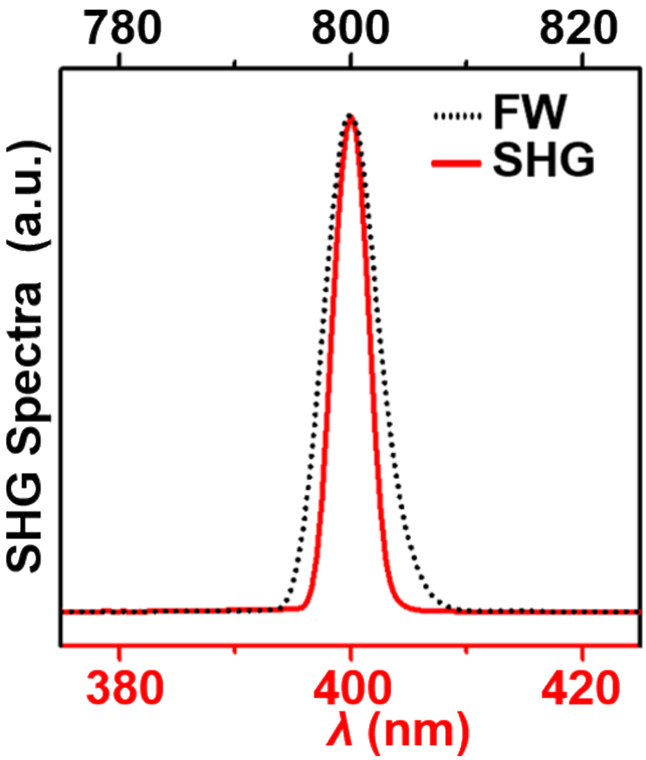

Figure S8. Comparing spectra profile of second harmonic generation with central wavelength of 400 nm (SHG, red line, bottom axis) and fundamental wave (FW, black dot, top axis) with central wavelength of 800 nm. To facilitate this comparison, the intensity is normalized. Compared with the FW, SHG spectrum is not broadened but slightly narrowed down. This is because the FW intensity is weakened at wavelength deviating from the central wavelength, which cannot be efficiently used to generate second harmonic signal.

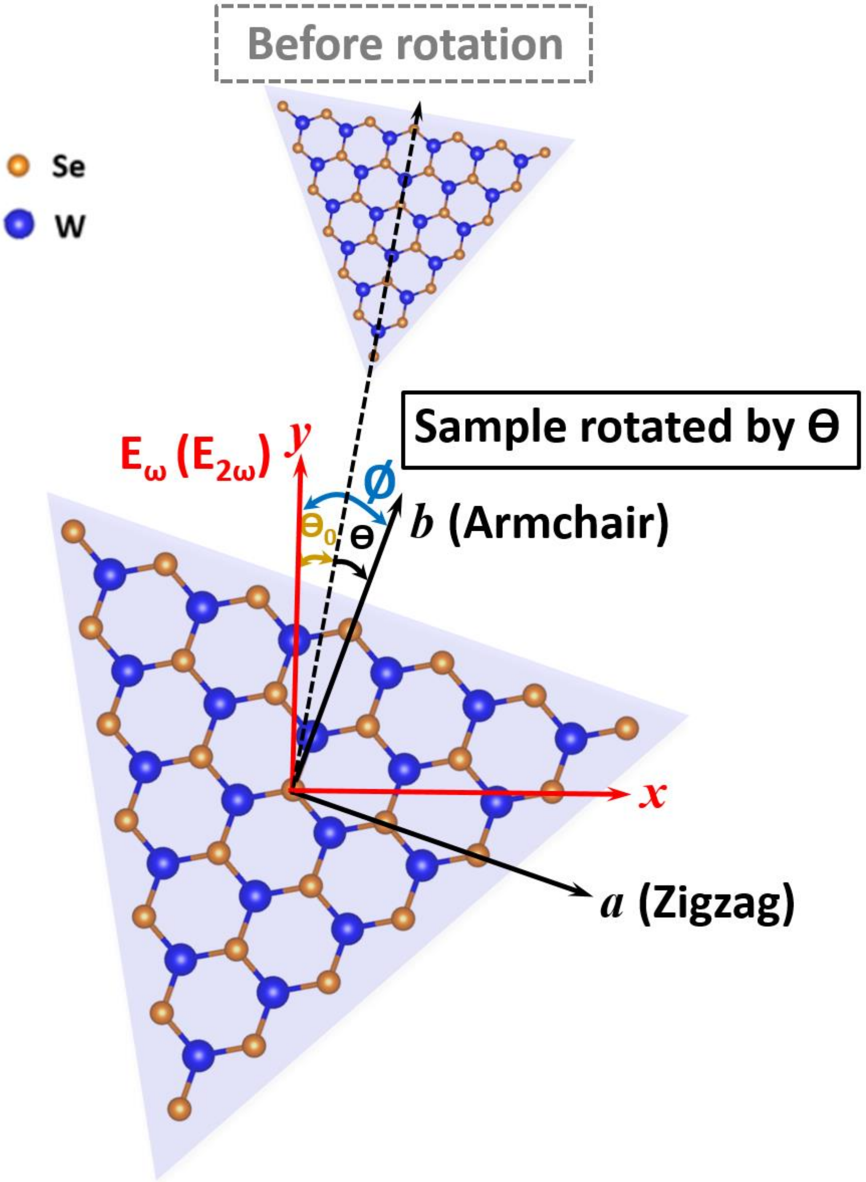

Figure S9. Demonstration of transformation from crystal coordinates (*a*, *b*, *c*) to laboratory coordinates (*x*, *y*, *z*). *a* and *b* denote the principle axes in the monolayer plane with *a* long the zigzag direction and *b* along the armchair direction. *c* is the principal axis along the out-of-plane 3-fold (C_3) rotation axis. In the laboratory coordinates, *x* is perpendicular to *y*. *y* is along the polarization direction of the pump laser and *z* is along the C_3 rotation axis. Triangle-shape monolayer WSe_2 flake (light blue) is composed of W atoms (blue) and Se atoms (yellow). In the initial position, the angle between the armchair direction of the WSe_2 flake and *y* axis is Θ_0. As the flake is rotated a degree of Θ, the angle between the armchair direction (*b*) of the WSe_2 flake and *y* axis becomes $\Theta_0+\Theta$, that is denoted as $\varnothing$.

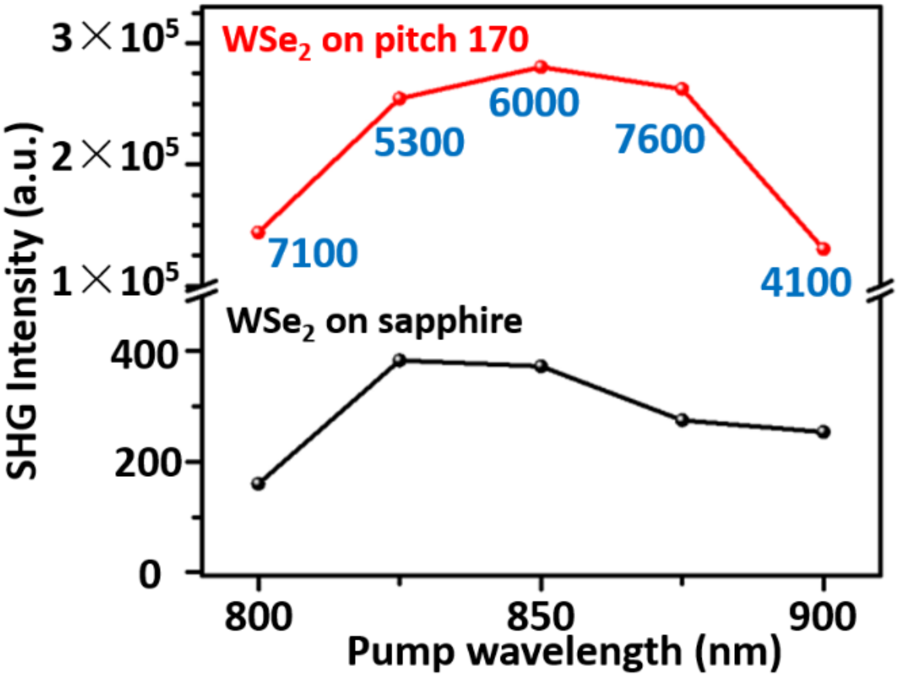

Figure S10. SHG intensity from monolayer WSe_2 on trenches with a pitch of 170 nm and on sapphire as a function of pump wavelength ranging from 800 nm to 900 nm. The blue numbers represent the enhancement factors of SHG (normalized by the trenches occupation) from the WSe_2 on trenches as compared with that of WSe_2 on sapphire for each pump wavelength.

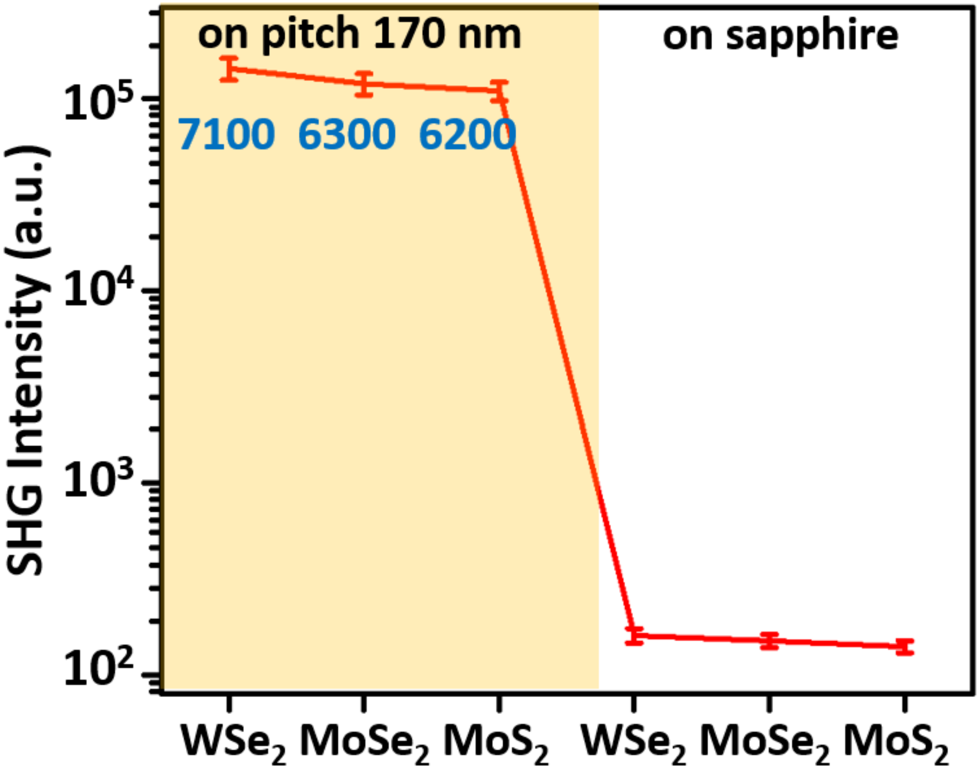

Figure S11. Quantitative comparison of SHG from monolayer WSe_2, $MoSe_2$ and MoS_2 on trenches with a pitch of 170 nm and on the as-grown sapphire. The pump laser is 800 nm. The blue numbers represent the enhancement factors of SHG (normalized by the trenches occupation) from the TMDCs on trenches.

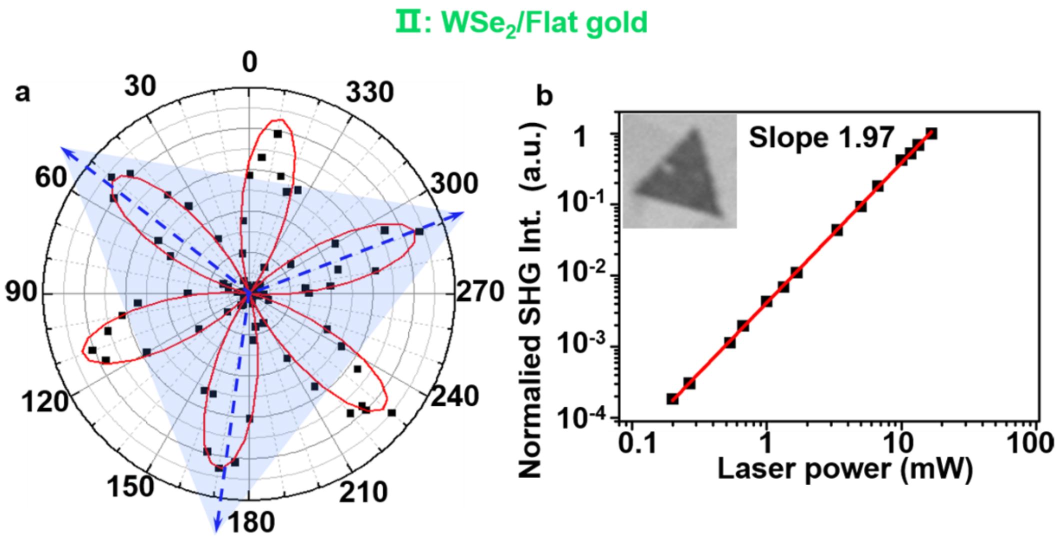

Figure S12. Dependence of the SHG on the sample rotated angle, laser power and pump wavelength on SHG intensity, respectively. (a) Polar plot of the normalized SHG intensity from (Ⅱ). The black squares are experimental data with fits shown in red according to the symmetry analysis in the text. The light blue triangle with dark blue dashed arrows is used to denote the crystal orientation. (b) Normalized SHG intensity from Ⅱ as a function of laser power in log-log scale plot.

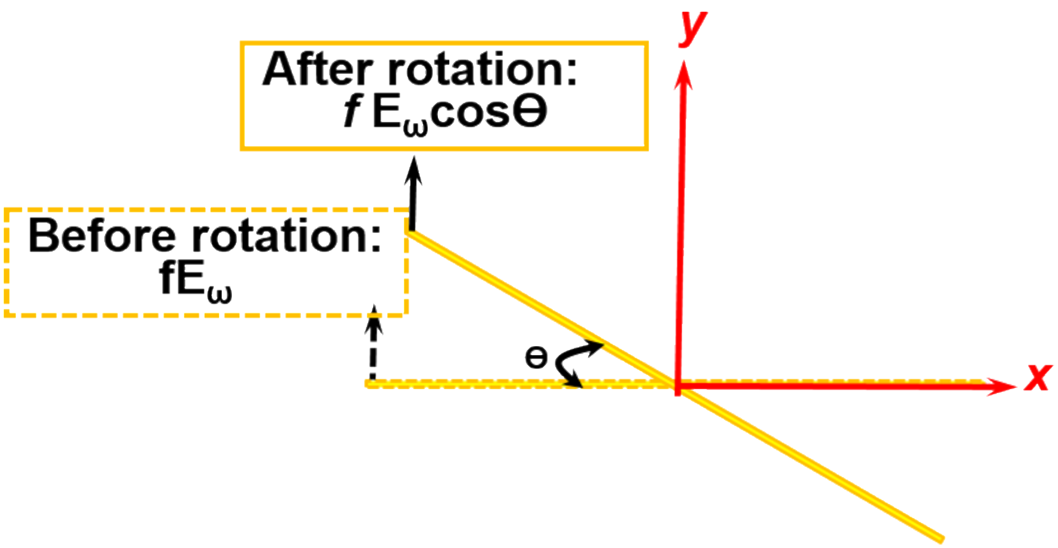

Figure S13. Demonstration of the electric field amplitude as a function of the rotation angle Θ of the trenches. In the initial position, the electric field over the trench is maximum with an enhancement factor of f, reaching a value of fE_ω. As the trench is rotated Θ, the electric field becomes $fE_\omega\cos\Theta$.

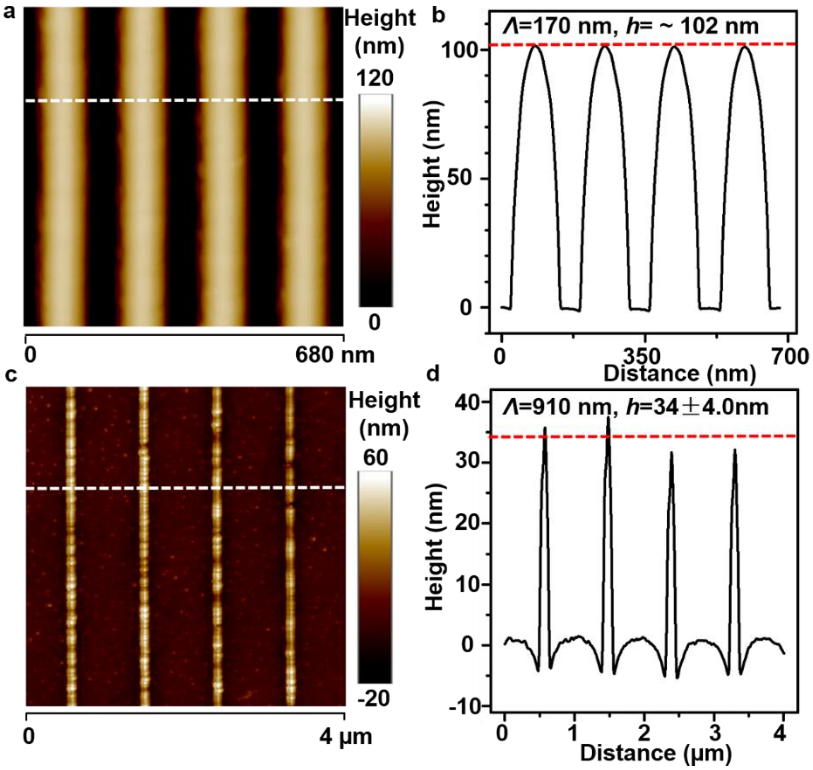

Figure S14. Height of the ridges on silicon template. AFM measurements of the patterned silicon template with pitch of 170 nm (a) and 910 nm (c). (b,d) The associated height profile along the white dashed lines in (a) and (c), respectively.

Supplementary Note

Supplementary Note 1 | Optical setup for SHG measurement

Figure S3 demonstrates the optical setup for the SHG experiments of WSe_2 on gold substrates at room temperature. A linearly polarized femtosecond laser with a central wavelength of 800 nm, repetition rate of 80 MHz and pulse duration of 140 fs, generated from a Ti: sapphire oscillator (Coherent, Chameleon Ultra Ⅱ), was focused on the sample through a 100× air objective with a numerical aperture (NA) of 0.90 (Nikon, Ti-U inverted microscope, TU Plan Fluor). The experiment of SHG as a function of pump wavelength (Figure S10) was using this laser with a central wavelength of 800, 825, 850, 875 or 900 nm. The sample was raster scanned by a piezo-actuated 3D nanopositioning stage (Physik Instrumente, P545.2R7). At each pixel, the back scattered SHG signal was collected through the same objective, and passed through a dichroic mirror (Semrock, FF750-SDi02-25×36) and a short-pass filter (Laser 2000, FF01-750/SP-25), which completely filtered out the pump laser before being detected by either a photomultiplier tube (PicoQuant, PMA 182) or a spectrometer (Princeton Instruments, 2300i).

Supplementary Note 2 | Normalization method of SHG from WSe$_2$ over the trenches.

As shown in Figure S7, the area ratio between the hot-spot area and the laser spot one was calculated in order to calculate the SHG enhancement factor of monolayer WSe$_2$ above the trenches. When the incident optical field is polarized along *x*-direction, the hot-spot area will be determined by the trenches within the laser spot. The laser spot is represented by the red circle with a radius of R (*i.e.* ~ 600 nm) with center point denoted as "O". The pitch size Λ of the structure is 170 nm and the maximum width of the trench W is 18 nm. The hot-spot area A_{gap} can then be calculated by:

$$A_{\text{gap}} = 4 \times W \times [\left(R + \sqrt{R^2 - \Lambda^2} + \sqrt{R^2 - (2\Lambda)^2} + \sqrt{R^2 - (3\Lambda)^2}\right), \tag{S1}$$

where A_{gap} is calculated to be 1.43×10^5 nm^2 and the laser spot area A_0 is $\pi \times 600^2$ nm^2. Thus, the area ratio of A_{gap}/A_0 calculated by this approach is 12.6%. The SHG enhancement factor of WSe$_2$ over the trench is scaled by multiplying the reciprocal of this ratio. This normalization method is also widely used. [S1, 3]

Supplementary Note 3 | Calculation of effective second-order susceptibility.

The susceptibility is calculated based on Andrea Alu's and Mikhail A. Belkin's method: [S5-6]

$$\chi_{eff}^{(2)} = \frac{(I_{2\omega})^{1/2}}{I_{\omega}} \bullet \frac{\sqrt{8\varepsilon_0 c^3}}{2\omega L}, \tag{S2}$$

where $\chi_{eff}^{(2)}$ includes local field enhancement at fundamental wavelength, I_{ω} and $I_{2\omega}$ are the pump laser and second-harmonic intensities, respectively, ε_0 is the dielectric constant in the vacuum, c is the light velocity in the vacuum, ω is the angular frequency of pump laser and L is the thickness of the monolayer WSe_2 (6.8 nm) which is far less than the coherent length. The intensity (I_{ω} and $I_{2\omega}$) is related with the peak power (P_{ω} and $P_{2\omega}$) by:

$$I_{\omega} = \frac{2P_{\omega}}{\pi R_{\omega}^2}, \tag{S3}$$

$$I_{2\omega} = \frac{2P_{2\omega}}{\pi R_{2\omega}^2}, \tag{S4}$$

where P_{ω} is the peak power of the pulsed laser with Gaussian profile, duration of D=140 fs and repetition rate of R=80 MHz, P_{ω} is the peak power of the second harmonic wave, R_{ω} is the radius of the pump laser, $R_{2\omega}$ is the radius of the second harmonic wave. The peak power P_{ω} and $P_{2\omega}$ are given by:

$$P_{\omega} = \frac{\overline{P_{\omega}}}{\mathrm{D}\cdot\mathrm{R}}, \tag{S5}$$

$$P_{2\omega} = \frac{\overline{P_{2\omega}}}{\mathrm{D}\cdot\mathrm{R}}, \tag{S6}$$

where $\overline{P_{\omega}}$ is the average power of the pump laser which can be directly measured by power meter and $\overline{P_{2\omega}}$ is the average power of the second harmonic signal which can be calculated by the following method. We calculated the SH power by building a relation between the signal power and number of counts per second as shown in the spectrometer. We fist illuminated 400-nm laser with known average power on a silver mirror (97% reflectance) and recorded the reflected signal by the spectrometer in the unit of counts, then we recorded the SH signal from our sample. By comparing the number of counts per second of these two signals, we can calculate the average power of the SH signal ($\overline{P_{2\omega}}$). With eqs S2-S6, the effective susceptibility $\chi_{eff}^{(2)}$ for monolayer WSe_2 on trenches and on sapphire is calculated to be ~ 2.1×10^4 pm/V with normalization of the trench occupation and ~ 248 pm/V, respectively.

Supplementary Note 4 | Influence of the crystal orientation on the SHG intensity.

We first derive general expressions for the principle of SHG, then provide the specific expressions for SHG from monolayer WSe_2 on trenches. When a fundamental laser with frequency ω illuminates the sample, a second-harmonic wave at frequency 2ω can be generated with a second-harmonic polarization ($\mathbf{P}_{i,2\omega}$) given by

$$\mathbf{P}_{i,2\omega} = \sum_j \sum_k \chi^{(2)}_{ijk}\, \mathbf{E}_{j,\omega}\mathbf{E}_{k,\omega}, \tag{S7}$$

where $(i, j, k) \in$ principle axes in crystal coordinate (a, b, c) with a representing the zigzag direction, b representing the armchair direction and c representing the out-of-plane 3-fold rotation axis (Figure S9). According to eq S7, it can be derived:

$$\begin{aligned}\mathbf{P}_{i,2\omega} = {} & \chi^{(2)}_{iaa}\, \mathbf{E}_{a,\omega}\mathbf{E}_{a,\omega} + \chi^{(2)}_{iab}\, \mathbf{E}_{a,\omega}\mathbf{E}_{b,\omega} + \chi^{(2)}_{iac}\, \mathbf{E}_{a,\omega}\mathbf{E}_{c,\omega} \\ & + \chi^{(2)}_{iba}\, \mathbf{E}_{b,\omega}\mathbf{E}_{a,\omega} + \chi^{(2)}_{ibb}\mathbf{E}_{b,\omega}\mathbf{E}_{b,\omega} + \chi^{(2)}_{ibc}\mathbf{E}_{b,\omega}\mathbf{E}_{c,\omega} \\ & + \chi^{(2)}_{ica}\, \mathbf{E}_{c,\omega}\mathbf{E}_{a,\omega} + \chi^{(2)}_{icb}\mathbf{E}_{c,\omega}\mathbf{E}_{b,\omega} + \chi^{(2)}_{icc}\mathbf{E}_{c,\omega}\mathbf{E}_{c,\omega}\end{aligned} \tag{S8}$$

The electric field of the fundamental laser is in the monolayer plane, so $|\mathbf{E}_{c,\omega}| = 0$.

$$\begin{cases} \mathbf{P}_{a,2\omega} = \chi^{(2)}_{aaa}\, \mathbf{E}_{a,\omega}\mathbf{E}_{a,\omega} + \chi^{(2)}_{aab}\, \mathbf{E}_{a,\omega}\mathbf{E}_{b,\omega} + \chi^{(2)}_{aba}\, \mathbf{E}_{a,\omega}\mathbf{E}_{b,\omega} + \chi^{(2)}_{abb}\, \mathbf{E}_{b,\omega}\mathbf{E}_{b,\omega} \\ \mathbf{P}_{b,2\omega} = \chi^{(2)}_{baa}\, \mathbf{E}_{a,\omega}\mathbf{E}_{a,\omega} + \chi^{(2)}_{bab}\, \mathbf{E}_{a,\omega}\mathbf{E}_{b,\omega} + \chi^{(2)}_{bba}\, \mathbf{E}_{a,\omega}\mathbf{E}_{b,\omega} + \chi^{(2)}_{bbb}\, \mathbf{E}_{b,\omega}\mathbf{E}_{b,\omega} \\ \mathbf{P}_{c,2\omega} = \chi^{(2)}_{caa}\, \mathbf{E}_{a,\omega}\mathbf{E}_{a,\omega} + \chi^{(2)}_{cab}\, \mathbf{E}_{a,\omega}\mathbf{E}_{b,\omega} + \chi^{(2)}_{cba}\, \mathbf{E}_{a,\omega}\mathbf{E}_{b,\omega} + \chi^{(2)}_{cbb}\, \mathbf{E}_{b,\omega}\mathbf{E}_{b,\omega} \end{cases} \tag{S9}$$

Given the monolayer WSe_2 belongs to the point group of D_{3h} ($\bar{6}m2$), the nonzero components are listed here with a relation as:

$$\chi^{(2)}_{bbb} = -\chi^{(2)}_{baa} = -\chi^{(2)}_{aba} = -\chi^{(2)}_{aab}. \tag{S10}$$

According to eqs S9-S10:

$$\begin{cases} \mathbf{P}_{a,2\omega} = \chi^{(2)}_{aab}\, \mathbf{E}_{a,\omega}\mathbf{E}_{b,\omega} + \chi^{(2)}_{aba}\, \mathbf{E}_{a,\omega}\mathbf{E}_{b,\omega} = -2\chi^{(2)}_{bbb}\, \mathbf{E}_{a,\omega}\mathbf{E}_{b,\omega} \\ \mathbf{P}_{b,2\omega} = \chi^{(2)}_{baa}\, \mathbf{E}_{a,\omega}\mathbf{E}_{a,\omega} + \chi^{(2)}_{bbb}\, \mathbf{E}_{b,\omega}\mathbf{E}_{b,\omega} = \chi^{(2)}_{bbb}\, (-\mathbf{E}_{a,\omega}\mathbf{E}_{a,\omega} + \mathbf{E}_{b,\omega}\mathbf{E}_{b,\omega})\cdot \\ \mathbf{P}_{c,2\omega} \propto 0 \end{cases} \tag{S11}$$

The components of the second-order nonlinear susceptibility are normally given in terms of the crystal axes, whereas it is convenient to describe the nonlinear polarization in terms of the laboratory axes as the direction of propagation and polarizations of the interacting waves are defined relative to the laboratory axes. Therefore, $\mathbf{P}$, $\chi^{(2)}$ and $\mathbf{E}$ elements expressed in the crystal coordinates (a, b, c) must be transformed to these in laboratory coordinates (x, y, z). Figure S9 demonstrates the relation between the crystal coordinate (a, b, c) and laboratory coordinate (x, y, z) in monolayer WSe_2. When y axis is at an angle $\varnothing$ from the b axis, there are:

$$\vec{a}.\vec{x} = cos\varnothing,\ \vec{b}.\vec{x} = sin\varnothing,\ \vec{a}.\vec{y} = -sin\varnothing,\ \vec{b}.\vec{y} = cos\varnothing. \tag{S12}$$

According to eqs S11-S12, we can obtain:

$$\mathbf{P}_{x,2\omega} = \mathbf{P}_{a,2\omega}\vec{a}.\vec{x} + \mathbf{P}_{b,2\omega}\vec{b}.\vec{x}$$

$$= -2\chi^{(2)}_{bbb}\, \mathbf{E}_{a,\omega}\mathbf{E}_{b,\omega} cos\varnothing + \chi^{(2)}_{bbb}\, (-\mathbf{E}_{a,\omega}\mathbf{E}_{a,\omega} + \mathbf{E}_{b,\omega}\mathbf{E}_{b,\omega}) sin\varnothing \tag{S13.1}$$

$$\mathbf{P}_{y,2\omega} = \mathbf{P}_{a,2\omega}\vec{a}.\vec{y} + \mathbf{P}_{b,2\omega}\vec{b}.\vec{y}$$

$$\propto 2\chi^{(2)}_{bbb}\, \mathbf{E}_{a,\omega}\mathbf{E}_{b,\omega} sin\varnothing + \chi^{(2)}_{bbb}\, (-\mathbf{E}_{a,\omega}\mathbf{E}_{a,\omega} + \mathbf{E}_{b,\omega}\mathbf{E}_{b,\omega}) cos\varnothing \tag{S13.2}$$

As the pump laser has electric field ($\mathbf{E}_\omega$) polarized along y axis, we can obtain:

$$\mathbf{E}_{a,\omega} = \mathbf{E}_\omega \vec{y}.\vec{a} = -\mathbf{E}_\omega sin\varnothing \tag{S14.1}$$

$$\mathbf{E}_{b,\omega} = \mathbf{E}_\omega \vec{y}.\vec{b} = \mathbf{E}_\omega cos\varnothing \tag{S14.2}$$

Substituting eqs S14.1 and S14.2 into eqs S13.1 and S13.2, we can obtain:

$$\mathbf{P}_{x,2\omega} = 2\chi^{(2)}_{bbb}\mathbf{E}^2_\omega sin\varnothing cos^2\varnothing + \chi^{(2)}_{bbb}\mathbf{E}^2_\omega (cos^2\varnothing - sin^2\varnothing) sin\varnothing$$

$$= (\chi_{bbb}^{(2)} sin3\O)\mathbf{E}_{\omega}^{2} \qquad (S15.1)$$

$$\mathbf{P}_{y,2\omega} = -2\chi_{bbb}^{(2)}\mathbf{E}_{\omega}^{2} cos\O sin^{2}\O + \chi_{bbb}^{(2)}\mathbf{E}_{\omega}^{2}(cos^{2}\O - sin^{2}\O)cos\O$$

$$= (\chi_{bbb}^{(2)} cos3\O)\mathbf{E}_{\omega}^{2} \qquad (S15.2)$$

From eqs S15.1-S15.2, we can derive the total SHG intensity $I_{2\omega}$:

$$I_{2\omega} = C|\mathbf{E}_{2\omega}|^{2} \propto (|\mathbf{P}_{x,2\omega}|^{2} + |\mathbf{P}_{y,2\omega}|^{2}) \propto |\chi_{bbb}^{(2)}|^{2}|\mathbf{E}_{\omega}|^{4}, \qquad (S16)$$

where $\mathbf{E}_{2\omega}$ is the electric field of the second-harmonic frequency wave and C is a constant.

In the experiments as shown in Figure 5b and Figure S12a, we put an analyzer before the spectrometer with polarization parallel to the pump laser, so we only need to consider the parallel component of SHG signal relative to the polarization of the pump laser ($\mathbf{E}_{\omega}$), which is related with $\mathbf{P}_{y,2\omega}$. As such, the effective second-order susceptibility turns to be $\chi_{bbb}^{(2)} cos3\O$.

Next, we consider the case of rotating the WSe_2 flake on a flat gold substrate. Before the rotation of WSe_2 flake, there exists an angle of Θ_0, between the armchair direction (b_0) of WSe_2 flake and the polarization of pump laser (y axis). Now, if the WSe_2 flake on the gold substrate is rotated by Θ, the new angle $\O$ between the armchair direction of WSe_2 and the polarization of the pump laser is $\O = \Theta_0 + \Theta$.

As a result, for monolayer WSe_2 on the flat gold, the parallel component of SHG intensity is:

$$I_{2\omega,WSe_2\,on\,flat\,gold}^{\parallel} \propto |\mathbf{P}_{y,2\omega}|^{2} = \mathbf{E}_{\omega}^{4}|\chi_{bbb}^{(2)}|^{2}cos^{2}3\O \propto cos^{2}3(\Theta_0 + \Theta). \qquad (S17)$$

Supplementary Note 5 | Influence of the trench orientation on the SHG intensity.

Figure S13 demonstrates the electric field amplitude as a function of the rotation angle Θ of the trenches. For monolayer WSe_2 as placed on trenches with localized plasmon resonances, the electric field of pump laser in the trench is enhanced by a factor of f. In the initial position, the trenches are perpendicular to the polarization of pump laser, so the electric field localized by the trenches is:

$$\mathbf{E}^{\parallel}_{\text{gap,initial}} = f\mathbf{E}_{\omega}. \tag{S18}$$

If the trenches have an angle of Θ with respect to the perpendicular direction of the pump laser polarization, *i.e.*, x axis, this electric field becomes:

$$\mathbf{E}^{\parallel}_{\text{gap,rotated}} = f\mathbf{E}_{\omega}cos\Theta. \tag{S19}$$

Therefore,

$$I^{\parallel}_{2\omega,WSe_2\ on\ trenches} \propto |\mathbf{P}_{y,2\omega}|^2 = |\chi^{(2)}_{bbb}|^2 cos^2 3\emptyset.(f\mathbf{E}_{\omega}cos\Theta)^4 \propto cos^2 3(\Theta_0 + \Theta)cos^4\Theta. \tag{S20}$$

Supplementary References

(1). Wang, Z.; Dong, Z.; Gu, Y.; Chang, Y.-H.; Zhang, L.; Li, L.-J.; Zhao, W.; Eda, G.; Zhang, W.; Grinblat, G. Giant Photoluminescence Enhancement in Tungsten-Diselenide–Gold Plasmonic Hybrid Structures. *Nat. Commun.* **2016,** *7*, 11283.

(2). Schwarz, S.; Dufferwiel, S.; Walker, P.; Withers, F.; Trichet, A.; Sich, M.; Li, F.; Chekhovich, E.; Borisenko, D.; Kolesnikov, N. N. Two-Dimensional Metal–Chalcogenide Films in Tunable Optical Microcavities. *Nano Lett.* **2014,** *14*, 7003-7008.

(3). Akselrod, G. M.; Ming, T.; Argyropoulos, C.; Hoang, T. B.; Lin, Y.; Ling, X.; Smith, D. R.; Kong, J.; Mikkelsen, M. H. Leveraging Nanocavity Harmonics for Control of Optical Processes in 2D Semiconductors. *Nano Lett.* **2015,** *15*, 3578-3584.

(4). Dong, Z.; Asbahi, M.; Lin, J.; Zhu, D.; Wang, Y. M.; Hippalgaonkar, K.; Chu, H.-S.; Goh, W. P.; Wang, F.; Huang, Z. Second-Harmonic Generation from Sub-5 nm Gaps by Directed Self-Assembly of Nanoparticles onto Template-Stripped Gold Substrates. *Nano Lett.* **2015,** *15*, 5976-5981.

(5). Lee, J.; Tymchenko, M.; Argyropoulos, C.; Chen, P.-Y.; Lu, F.; Demmerle, F.; Boehm, G.; Amann, M.-C.; Alu, A.; Belkin, M. A. Giant Nonlinear Response from Plasmonic Metasurfaces Coupled to Intersubband Transitions. *Nature* **2014,** *511*, 65-69.

(6). Gomez-Diaz, J. S.; Tymchenko, M.; Lee, J.; Belkin, M. A.; Alù, A. Nonlinear Processes in Multi-Quantum-Well Plasmonic Metasurfaces: Electromagnetic Response, Saturation Effects, Limits, and Potentials. *Phys. Rev. B* **2015,** *92*, 125429.